Correlation between Photovoltaic Performance and Impedance Spectroscopy of Dye-Sensitized Solar Cells Based on Ionic Liquids

Francisco Fabregat-Santiago,*,† Juan Bisquert,† Emilio Palomares,‡ Luis Otero,§ Daibin Kuang,‖ Shaik M. Zakeeruddin,‖ and Michael Grätzel*,‖

Departament de Física, Universitat Jaume I, Avinguda Vicent Sos Baynat s/n, 12071 Castelló, Spain, Institute of Chemical Research of Catalonia (ICIQ), Avinguda Països Catalans 16, 43007 Tarragona, Spain, Departamento de Química, Universidad Nacional de Río Cuarto, Agencia Postal 3 (5800), Río Cuarto, Argentina, and Laboratory for Photonics and Interfaces, Institute of Chemical Sciences and Engineering, Ecole Polytechnique Federale de Lausanne, 1015 Lausanne, Switzerland

In this work, we study the characteristics of dye-sensitized solar cells using an ionic liquid as the electrolyte and compare them with the response of a solvent-containing electrolyte cell. Impedance spectroscopy is used to derive the key circuit elements determining the photovoltaic performance of the cell. On the basis of this data, photocurrent voltage curves are calculated and compared with experimental results.

1. Introduction

Dye-sensitized solar cells[1] (DSCs) have attracted much attention in the research for an alternative and low-cost energy source. Over 11% efficiency has been reached with the use of organic electrolytes as hole conducting media.[2,3] However volatility of the solvents employed is a major issue for the implementation in long-life devices.[4,5] Several options are being investigated to substitute the organic solvent-containing electrolyte by a solid or low volatility phase.[6−10] In this respect, recent works on the use of room-temperature ionic liquids (RTILs) for dye-sensitized solar cells (DSCs) is particularly relevant.[11−13]

RTILs are promising for many electrochemical systems such as actuators, batteries, supercapacitors, electrochromic windows, displays, photovoltaic cells, and light-emitting electrochemical cells. From the electrochemical point of view, ionic liquids have excellent properties: they exhibit high-ionic conductivity and wide potential windows.[14−20] Furthermore, they are nonvolatile, nonflammable, and have high thermal stability, making them especially suitable for long term outside DSC applications avoiding problems such as leakage and evaporation of the organic solvent that are notorious for conventional solvent-containing electrolytes.

In the study of DSCs, classical diode models applied in solid-state solar cells are also used.[21] However, interpretation of the parameters obtained from these models and their relationship with the physical chemistry fundamental processes governing the performance of the cell is not always provided. Recent works based on impedance spectroscopy have described the effect on the i−V characteristics of several interfacial charge-transfer and transport mechanisms occurring in DSC.[21−26] In this work, we associate all the characteristic electrochemical processes occur-

ring in liquid electrolyte and ionic liquid based DSCs with their effect on the factors that govern the efficiency of the device and we rebuild the i−V curve of the solar cells from impedance data and relate them with the elements in the classical solar cell models.

It is important to determine in detail the operational properties of the DSCs with RTILs, since their performance has not yet reached that of the DSCs-containing organic electrolytes. This study employs impedance spectroscopy as a tool to scrutinize the salient factors governing the performance of RTIL-based DSCs. The central emphasis of this work is to identify the key electric circuit elements determining the steady-state functioning of the solar cells and to explore what may be done to improve them. We shall also compare two different RTIL compositions with the behavior of DSCs based on standard liquid electrolyte.

2. Experimental Section

Electrochemical measurements were carried out in a two-electrode configuration, keeping always the platinized electrode as counter-electrode. Impedance and voltammetry experiments were performed on an Autolab general purpose electrochemical (AUT30.FRA2-AUTOLAB, Eco Chemie, B.V., The Netherlands).

Table 1 presents the configurations and photovoltaic parameters of the cells measured. Blank samples with RTIL sandwiched between asymmetric transparent-conducting oxide (TCO) and Pt-activated TCO and symmetric Pt-activated TCO electrodes (spacers before melting 25 μm thick) were used to measure electrical properties of the mixed ionic liquid electrolyte Z380 (*N*-methylbenzimidazole, nMBI, 0.5 M, guanidinium thiocyanate 0.12 M, and iodine (I$_2$) 0.2 M in 1-methyl-3-propylimidazolium iodide and 1-methyl-3-ethylimidazolium thiocyanate, 65:35 percent volume ratio) and the pure ionic salt electrolyte Z594 (nMBI 0.5 M, and I$_2$ 0.2 M in 1-methyl-3-propylimidazolium iodide, MPII).

DSCs were prepared from a 6.8 μm nanoporous TiO$_2$ (n-TiO2) plus a scattering layer of 4 μm deposited on fluorine-doped tin oxide glass (FTO-glass). The K-19 dye[27] was employed as a sensitizer and was adsorbed from a solution of

* Corresponding authors. (F.F.S.) E-mail: fabresan@fca.uji.es. Tel.: +34-964-728024. Fax: +34-964-729218. (M.G.) E-mail: michael.graetzel@epfl.ch.
† Universitat Jaume I.
‡ Institut Català d'Investigació Química.
§ Universidad Nacional de Río Cuarto.
‖ Ecole Polytechnique Federale de Lausanne.

Impedance Spectroscopy of Dye-Sensitized Solar Cells

J. Phys. Chem. C, Vol. 111, No. 17, 2007 **6551**

TABLE 1: Sample Configuration and *j*−V Characteristics at 1 Sun AM 1.5 Illumination

sample	configuration	J_{sc} (mA cm^{-2})	V_{oc} (V)	FF	η (%)
Z380	TCO//Z380//Pt				
Z594	TCO//Z594//Pt				
P380	Pt//Z380//Pt				
P594	Pt//Z594//Pt				
C325	TCO//n−TiO2 + dye//Z325//Pt	17.06	0.762	0.72	9.64
C380	TCO//n−TiO2 + dye//Z380//Pt	13.99	0.707	0.71	7.05
C594	TCO//n−TiO2 + dye//Z594//Pt	13.07	0.678	0.71	6.27

a mixture of acetonitrile/*t*-butanol (50/50 v/v) along with phenylproprionic acid (PPA) as a coadsorbent, both having a concentration of 5×10^{-4} M. Apart from the two solvent-free ionic liquids, a solvent-based electrolyte, coded Z325, was employed containing 0.6 M 1-methyl-3-propylimidazolium iodide, 0.5 M *t*-butyl pyridine, and 0.03 M I$_2$ in a 3:1 mixture (v/v) of acetonitrile and valeronitrile. Characteristics of each sample are summarized in Table 1. All cells had an active area of 0.28 cm^2, and the samples were sealed with 25 μm hot melt spacers. Characteristic performance parameters of the cells in Table 1 were taken with a 0.16 cm^2 mask and a 1000 W xenon lamp filtered to AM 1.5 conditions. All the other electrochemical measurements were done using a 50 W halogen lamp as light source. Note that for these measurements, when we speak of 0.5 sun and 1 sun illumination we are referring to 500 W m^{-2} and 1000 W m^{-2} intense halogen light, respectively, but not to standard air mass 1.5 solar emission conditions. Viscosity measurements were carried out at 20 °C on a Haake microviscosimeter, VT 500 viscositester.

3. Results and Discussion

First we address the ionic conductivity of the RTILs. Figure 1 shows the *i*−V curve of Z594 electrolyte blank sample. Here the Z594 is contained in an asymmetric sandwich cell composed of two identical FTO glass electrodes, one being platinized (acting as working electrode) and the other not (being the counter and reference electrode). The characteristic mass-transfer limitation of the current is observed at high enough potentials, either positive or negative, the sign referring to the Pt-covered FTO electrode. This saturation of the current density, j_{lim}, due to the transport of the ionic carriers from one electrode to the other through the whole electrolyte allows to us calculate the diffusion coefficient of the I$_3^-$, as its concentration is much lower than I$^-$, in the cell by means of the expression[28,29]

$$D_{I_3^-} = \frac{l}{2nFc_{I_3^-}} j_{lim} \tag{1}$$

where $n = 2$ is the number of electrons involved in the electrochemical reduction of triiodide at the electrode, F is Faraday's constant, $c_{I_3^-}$ is the concentration per volume unit of I$_3^-$, assumed uniform along the whole cell, and l is the distance between the electrodes. Considering that all the I$_2$ added to the electrolyte is converted to I$_3^-$ and that $l \approx 20$ μm, electrolytes Z380 and Z594 yield $D_{I_3^-} = 3.0 \times 10^{-7}$ cm^2 s^{-1} and $D_{I_3^-} = 1.9 \times 10^{-7}$ cm^2 s^{-1}, respectively. The ratio of the diffusion coefficients agrees quite well with the difference in the viscosities of the two ionic liquids: 135 cPs for the mixed electrolyte and 285 cPs for the pure MPII electrolyte.

These values of diffusion coefficient show a first difference of the RTIL with respect to solvent-containing electrolytes as they are around 2 orders of magnitude lower than in acetonitrile. To avoid mass-transfer limitation of the photocurrent, it is
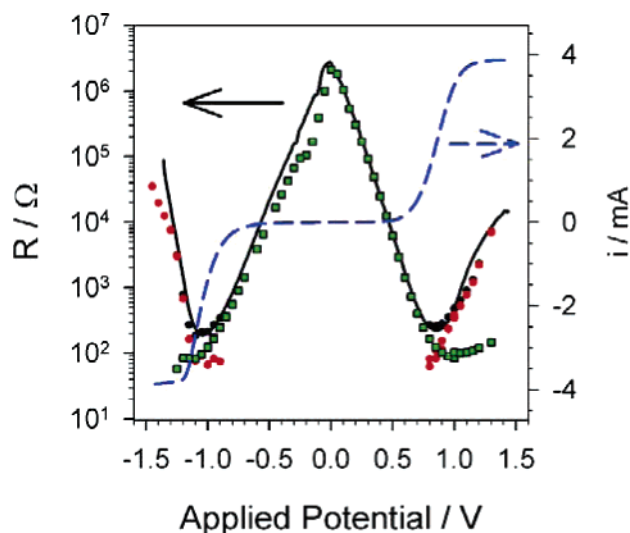

Figure 1. Left axis: the total resistance (black circles) and its different contributions of the Z594 blank cell with pure MPII ionic liquid electrolyte from impedance and the total resistance obtained from *i*−V curve (black line). The contribution from charge-transfer (green squares) dominates the central potentials plotted while diffusion resistance (red circles) dominates at the extremes, where high currents are passing through the cell. Right axis: the dashed blue line represents the *i*−V curve of the same cell.

necessary to reduce the film thickness and increase the triiodide concentration, although the latter brings about other losses due to light absorption by I$_3^-$ and enhanced dark currents.

At small applied potentials, however, the current limitation is due to the charge-transfer process from the electrodes (mainly the bare TCO) to the redox couple in the electrolyte. This may be observed in more detail in the impedance spectroscopy results shown in Figure 2. At intermediate potentials, the spectra show two arcs. The main contribution to the first (high frequency) semicircle arises from the parallel connection of the coupling between the Helmholtz capacities of both electrodes and the electron-transfer resistance of the bare TCO electrode. The charge-transfer resistance of the platinized TCO counter electrode was observed to be relatively small, presenting little changes with potential in comparison to bare TCO.[28] The second (low frequency) arc corresponds to the diffusion of I$_3^-$ (holes) in the electrolyte.

Figure 2b shows that the high-frequency arc augments in size with decreasing voltage, reflecting the increase in the charge-transfer resistance at the TCO electrolyte interface in the asymmetric cells. By contrast, the triiodide diffusion arc decreases in size and eventually merges with the growing charge-transfer semicircle. At cell potentials of 1 V and above, the diffusion arc dominates the overall spectrum leaving the interfacial charge-transfer effects as a small contribution at high frequencies (Figure 2c). As noted above, the symmetric blank cells present a smaller high-frequency arc, due to the joint contribution of both electrodes, that remained nearly constant at all the voltages applied (Figure 2d,e). This allows us to observe the characteristic low-frequency spectrum of impedance at all the potentials. When increasing the potential, the diffusion arc followed the same trend as for asymmetric blanks, and for similar currents passing through the blank cells the diffusion spectra presented the same aspect both in the asymmetric and symmetric configuration (Figure 2d,e).

Within a very good approximation, these impedance spectra may be modeled by a standard Randles equivalent circuit,[30] indicated in Figure 2a. R_{STCO} represents the series resistance of
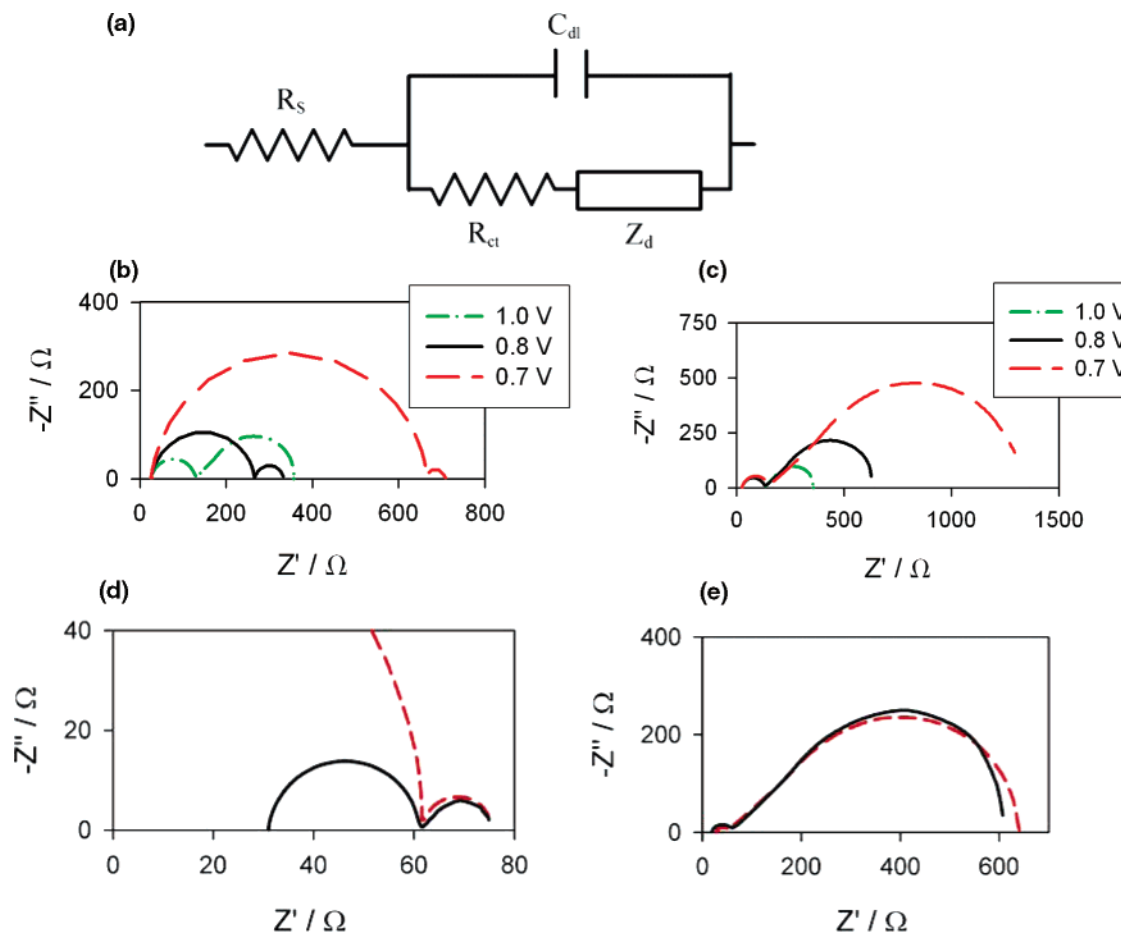
Figure 2. (a) Equivalent circuit of blank cells. (b) Impedance plot of asymmetric Z594 blank cell at several potentials in which the high-frequency arc corresponding to the parallel combination of R_{ct_c} and C_{dl} dominates. (c) The same in the region in which the low-frequency arc due to the diffusion impedance Z_d dominates. (d) Comparison of asymmetric (red dashed line) and symmetric (solid black line) cells at 0.6 and 0 V, respectively. The spectrum of the asymmetric cell has been displaced 340 Ω to to match the diffusion impedance. (e) The same as in (d) but at 1.1 V for the asymmetric and 0.3 V for the symmetric blank. No displacement has been used in this case.

leads and TCO (it is the resistance at which the first arc starts), R_{ct_c} is the sum of the charge-transfer resistances of both electrodes (the width of the first arc in Figure 2), C is the coupled capacitance mentioned above, and Z_d is the diffusion impedance given by

$$Z_d = R_d \frac{\tanh{(j\omega/\omega_d)}}{j\omega/\omega_d} \qquad (2)$$

where R_d is the diffusion resistance (the width of the second arc in Figure 2), $j = \sqrt{-1}$, ω is the angular frequency of measurement, and $\omega_d = D/L^2$, with D being the diffusion coefficient and L being the effective thickness of the film, which is taken as half of the thickness of the sample.[31] Data obtained in both configurations gave the same result and fit well to this model (see Supporting Information, Figure S.1). Using eq 2, we have calculated for electrolyte Z380, $D_{I_3^-} = 2.2 \times 10^{-7}$ cm^2 s^{-1}, and for electrolyte Z594, $D_{I_3^-} = 1.9 \times 10^{-7}$ cm^2 s^{-1}, which agree with the data obtained above from the steady-state measurements.

The knowledge of the diffusion resistance allows us to compare the results of impedance analysis with those from the $i-V$ curve. The derivative of the $i-V$ curve provides the overall resistance of the cell through

$$R_{total} = -\left(\frac{di}{dV}\right)^{-1} \qquad (3)$$

From Figure 1, the direct current (dc) and alternating current (ac) results match very well, given that different methods were employed to measure them.

There are two important features in Figures 1 and 2 that affect the application of RTIL in DSCs. The first, observed in Figure 2d, is that R_d presents a minimum value at 0 V in the symmetric blank. This is also suggested in Figure 1 at around −1 V for the asymmetric cell at which R_d tends to stabilize to the same threshold value. The characteristics of the impedance spectra do not allow to follow the behavior of diffusion resistance to lower potential values in the asymmetric cell. The second is that when the currents passing through the cell exceed a certain threshold value, in this case $i_t = 4$ mA/cm^2 at 18 °C, R_d tends to rise exponentially.

Figure 3 shows the impedance spectra change of a fully functioning DSC. A new arc appears at intermediate frequencies between that of the counter electrode and diffusion due to the contribution of the dye-sensitized nanocrystalline TiO$_2$ film component of the cell. At certain potentials, this intermediate arc completely dominates the impedance of the sample, and it is possible to recognize the characteristic shape of transport and recombination through the semiconductor[23] (Figure 3c). Note that although only one of the samples is shown here, this spectrum is observed for all of them.

The equivalent circuit of the complete cell may be then represented by a transmission line model as indicated in Figure 4a.[23,22] If we take L as the thickness of the nanoporous TiO$_2$

Impedance Spectroscopy of Dye-Sensitized Solar Cells

J. Phys. Chem. C, Vol. 111, No. 17, 2007 **6553**
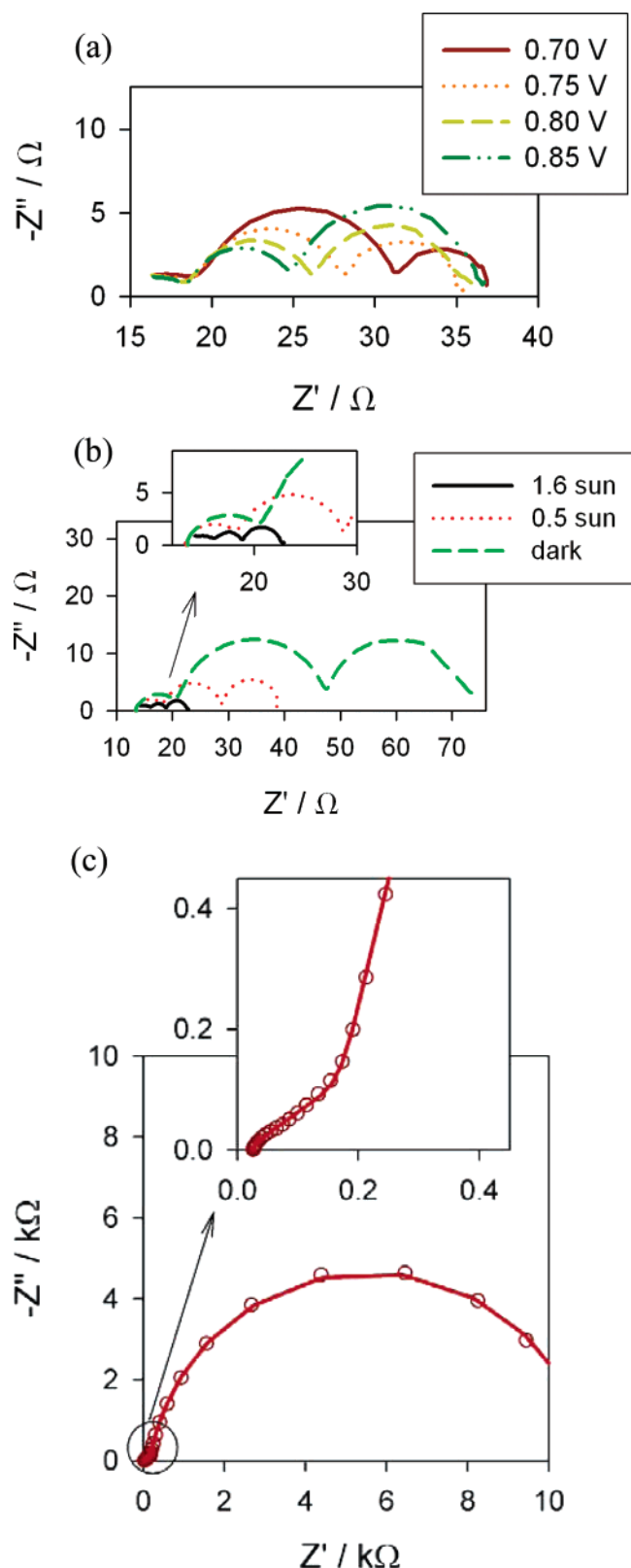
Figure 3. (a) Impedance spectra of sample complete DSC with the mixed RTIL, C380, at 1000 W cm^{-2} and different applied potentials. (b) The same sample polarized at 0.75 V and different illumination conditions. (c) At 0.5 V in the dark, the characteristic spectrum accounting for the transmission line equivalent circuit is observed. The straight line at high frequencies in the inset accounts for transport in TiO$_2$, while the big arc at low frequencies accounts for charge-transfer from TiO$_2$ to the electrolyte (charge losses).

film, the most characteristic elements of the transmission line are the electron transport resistance in TiO$_2$, R_t ($= r_t L$), the

interfacial charge recombination resistance $R_{ct_{TiO2}}$ ($= r_{ct}/L$), and the chemical capacitance produced by the accumulation of electrons in the film C_μ ($= c_\mu L$).[32] The other elements in the equivalent circuit model that describe additional processes in the DSC are the charge-transfer resistance R_{Pt} and the interfacial capacitance C_{Pt} at the platinized counter electrode/electrolyte interface, the charge-transfer resistance R_{TCO} for electron recombination from the uncovered layer of the TCO to the electrolyte, the sheet resistance R_S of the conducting glass (TCO), the capacitance C_{TCO} at the exposed FTO/electrolyte interface, the resistance R_{CO} and the capacitance C_{CO} at TCO/TiO$_2$ contact, and finally the impedance $Z_{d(sol)}$ with dc resistance R_d showing diffusion of the redox species in the electrolyte.

The shape and characteristic evolution of the impedance spectra and equivalent circuits of DSCs have been described in detail previously.[23,26] Under high-illumination intensity, the transport resistance becomes negligible and the complete equivalent circuit may be simplified as in Figure 4b.[23,24] At high potentials, the equivalent circuit of the working electrode further reduces to a simple arc generated by the chemical capacitance of TiO$_2$ in parallel with the charge-transfer resistance of TiO$_2$ to the electrolyte (the width of the central arc in Figure 3a,b), represented by $R_{ct_{TiO2}}$ in Figure 4b. On the other side, at the lower potentials the TiO$_2$ becomes an insulator and the impedance is dominated by the parallel combination of the double-layer capacitance at the bottom of the pores of the nanostructured matrix and the charge losses from TCO to electrolyte, $R_{ct_{TCO}}$. The overall charge-transfer resistance associated to the cell is then the parallel combination of both, $R_{ct} = R_{ct_{TCO}}||R_{ct_{TiO2}}$.

We will focus our attention on the evolution of the different resistances contributing to the total resistance of the sample, as they will determine the steady-state behavior of the system. Figure 3a shows Nyquist plots measured under 500 W/m^2 halogen light. The size of the low-frequency diffusion arc grows with forward bias (i.e., with increasing current). Meanwhile, $R_{ct_{TiO2}}$, the resistance of interfacial charge-transfer from the TiO$_2$ to the triiodide in the electrolyte, decreases due to the increase of the electron concentration in the TiO$_2$.[23] The high-frequency arc remains nearly constant. This arc is due to the coupling between the capacities of the counter electrode and the TCO/electrolyte interface at the bottom of the TiO$_2$ film (C_{co} is assumed to be negligible) with R_c, the resistance given by the sum of the counter electrode/electrolyte and TCO/TiO$_2$ interface[22] ($R_c = R_{Pt} + R_{co}$ is the width of this arc).

The effect of the light intensity on these parameters is shown in Figure 3b in which one sample is kept at -0.75 V under different illumination conditions. All the arcs strongly decrease in size with increasing light level. One of the reasons for this is the heating of the cell by the halogen lamp. The increase of temperature accelerates the interfacial charge-transfer in TiO$_2$ due to the inverse proportionality in eq 4 and also in R_{Pt} for the same reason. On the other side, this increase of temperature also reduces the viscosity of the electrolyte[33] and as a direct consequence diminishes the diffusion resistance, which is proportional to viscosity, and increases the diffusion coeficient (see Supporting Information).

The rise of the local triiodide ion concentration in the pores under illumination also contributes to the decrease of R_{ct} as it accelerates the recapture of conduction band electrons by the redox electrolyte. An additional effect of the light exposure is that the transport resistance of the TiO$_2$ film,[23] which is present in the dark, becomes negligible.

(a)

(b)
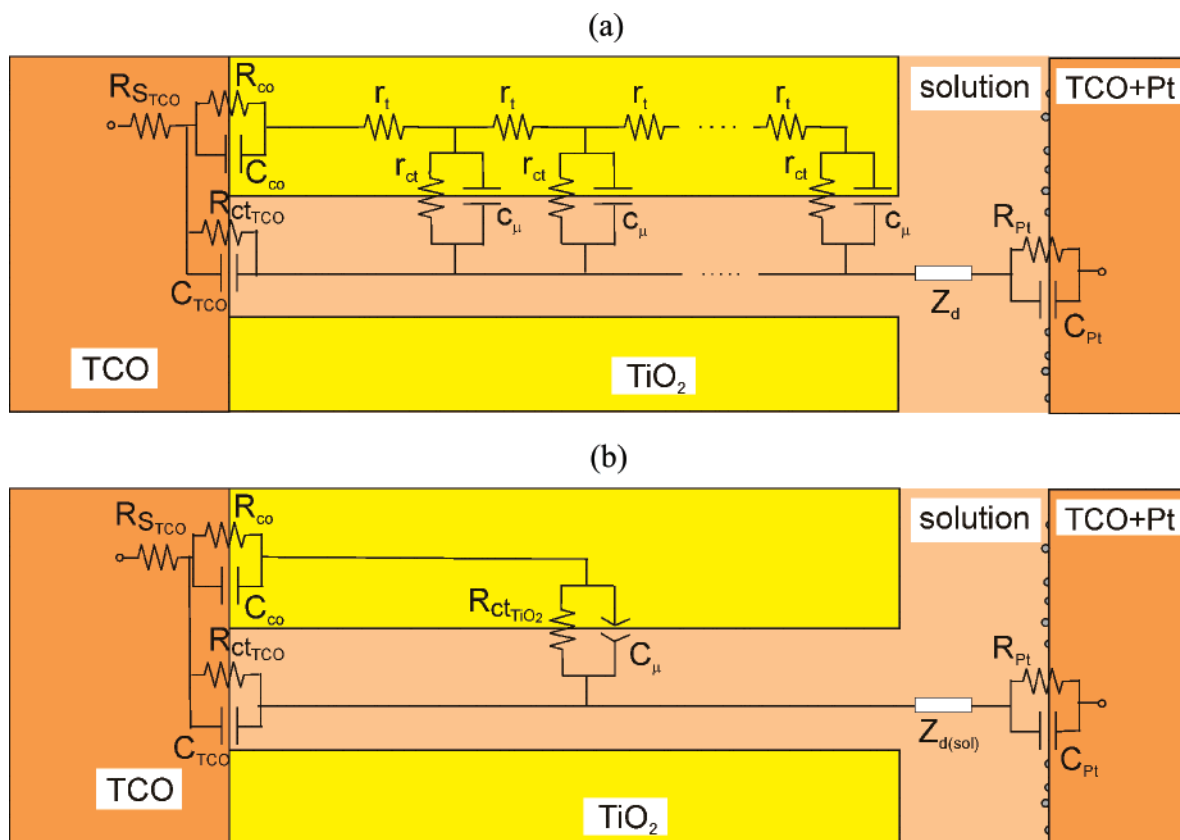
Figure 4. (a) General transmission line model of DSCs. The r_{ct} is the charge-transfer resistance of the charge recombination process between electrons in mesoscopic TiO$_2$ film and I$_3^-$ in electrolyte; c_μ is the chemical capacitance of TiO$_2$ film; r_t is the transport resistance of electrons in TiO$_2$ film; Z_d is the Warburg element showing the Nernst diffusion of I$_3^-$ in electrolyte; R_{Pt} and C_{Pt} are the charge-transfer resistance and double-layer capacitance at the counter electrode (platinized TCO glass); R_{TCO} and C_{TCO} are the charge-transfer resistance and the corresponding double-layer capacitance at exposed TCO/electrolyte interface; R_{CO} and C_{CO} are the resistance and the capacitance at TCO/TiO$_2$ contact; R_s is the series resistance, including the sheet resistance of TCO glass and contact resistance of the cell. L is the thickness of the mesoscopic TiO$_2$ film. (b) Simplified model at high illumination intensities.

Figure 5 shows the results of the measured diffusion resistance at these potentials, both in the dark and under 1000 W m^{-2} illumination, for the samples with the two different RTILs and the solvent-containing electrolyte cell. The comparison between the two kinds of cells shows clearly that the solvent-containing electrolyte has a lower R_d that furthermore changes more slowly than for the RTIL.

The dependency on the potential may be understood in terms of the data obtained previously for the blank cell (Figure 1). When the absolute value of the current increases, R_d rises. The minimum of R_d occurs when no net steady-state current is passing through the cells and when it is only given by the small ac modulation. Thus, this minimum provides a good estimation of the open circuit potential of the cell.

As pointed out above, the difference between dark and illumination is related to changes in temperature and local triiodide concentration in the pores. Exposure to a high-intensity halogen lamp lowers the viscosity of the ionic liquid[33] thereby increasing the diffusion coefficient obtained from the fit of impedance data, Table 2, and reducing R_d, Figure 5. The faster progression of the diffusion coefficient for the cell with the pure ionic liquid shown in Table 2 agrees well with the relatively bigger decrease in the value of the diffusion resistance of this sample with respect to the mixed ionic liquid one.

Comparison of charge-transfer, capacitance data, and recombination time obtained from impedance for the different samples are plotted in Figure 6 for the liquid, C325, and the different ionic salt electrolytes, C380 and C594, at 1000 W m^{-2} illumination.

The charge-transfer resistance of cells with ionic liquid, shown in Figure 6a, presents three regions. Below 0.35 V, charge-transfer is dominated by losses from FTO back-layer that still occur despite the coverage after treatment with TiCl$_4$. However, given the values they have at these potentials, these losses have a minor effect on the efficiency of the cell, even for the case of the liquid cell that presents smaller values probably because of a poorer quality on the back-layer.
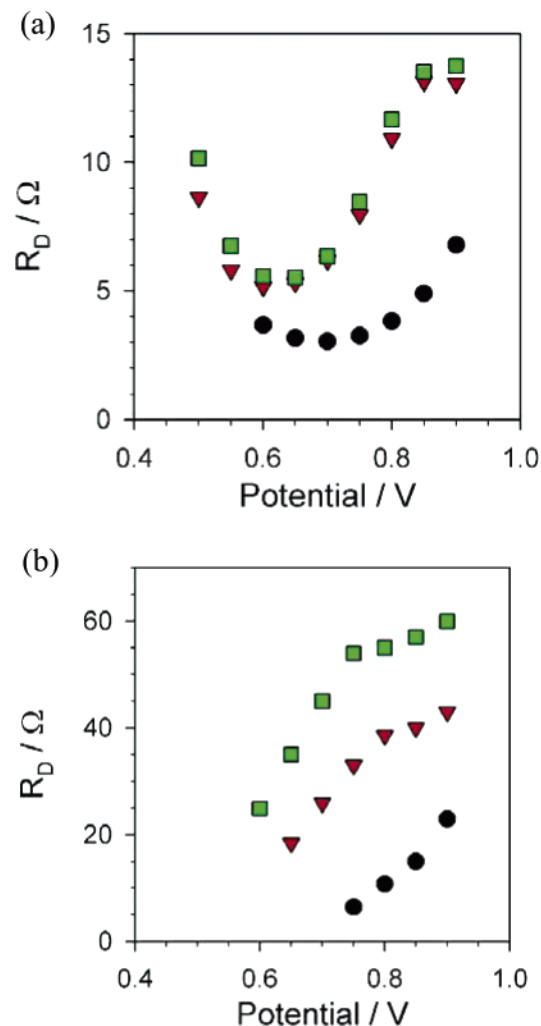
Above 0.35 V, the slope in the exponential potential dependence of charge-transfer of ionic liquid cells increases, indicating the change to the region in which charge-transfer from TiO$_2$ to electrolyte dominates the losses in the cell.

At the higher potentials, the slope decreases. This effect is due to the contribution of the series resistance of the cell that becomes of the same order of magnitude as charge-transfer resistance. Correcting for the potential drop produced by this series resistance, it is possible to extend the observation of R_{ct} for the real values of the potential in the electrode, Figure 7a. Furthermore, in the case of liquid cell C325 series resistance correction allows us to observe the transition from the region in which losses from FTO dominates to the one in which they are due to TiO$_2$.

Charge-transfer follows at moderate potentials the Buttler−Volmer relationship that yields to[23,34]

$$R_{ct} = \frac{1}{e}\left(\frac{dj_{rec}}{dE_{Fn}}\right)^{-1} = R_0 \exp\left[-\frac{\beta}{k_B T}(E_{Fn} - E_{redox})\right] \quad (4)$$

where j_{rec} is the recombination (or losses) current, E_{Fn} is the

Impedance Spectroscopy of Dye-Sensitized Solar Cells

J. Phys. Chem. C, Vol. 111, No. 17, 2007 **6555**

Figure 5. Diffusion resistance under 1000 W/m² illumination of DSCs (a) and in the dark (b) employing RTIL mixed Z380 (red inverted triangles), pure MPII Z594 (green squares), and liquid Z325 (black circles) electrolyte in the complete cells.

TABLE 2: Change in the Effective Diffusion Coefficient with Heat Produced by Illumination, Assuming That I_3^- Diffuses along the Whole Thickness of the Cell

cell	in dark	at 500 W m⁻²	at 1000 W m⁻²
C594	1.5×10^{-7} cm² s⁻¹	2.7×10^{-7} cm² s⁻¹	5.3×10^{-7} cm² s⁻¹
C380	2.5×10^{-7} cm² s⁻¹	4.8×10^{-7} cm² s⁻¹	8.3×10^{-7} cm² s⁻¹

position of the Fermi level of electrons, E_{redox} is the energy of the redox couple, $E_{Fn} - E_{redox} = eV$ where e is the electron charge and V the potential at the electrode, β is the transfer coefficient, R_0 is a constant, k_B is the Boltzman constant, and T is the absolute temperature.

Calculation of the transfer factor from TiO₂ recombination resistance gives $\beta = 0.78$ for the ionic liquids and $\beta = 0.70$ for the liquid electrolyte. An important result in Figure 7a is that at high potentials, the charge-transfer resistance of ionic liquid cells drops below the values of the liquid one. These larger charge losses limit the open circuit potential to lower values in ionic liquid cells, although ionic liquid cells have their conduction band at a slightly higher value than the liquid cell, as may be seen from the transport resistance in the dark shown in Figure 7b.

In the absence of illumination, evolution of transport resistance of electrons in TiO₂ may be observed in a wide enough
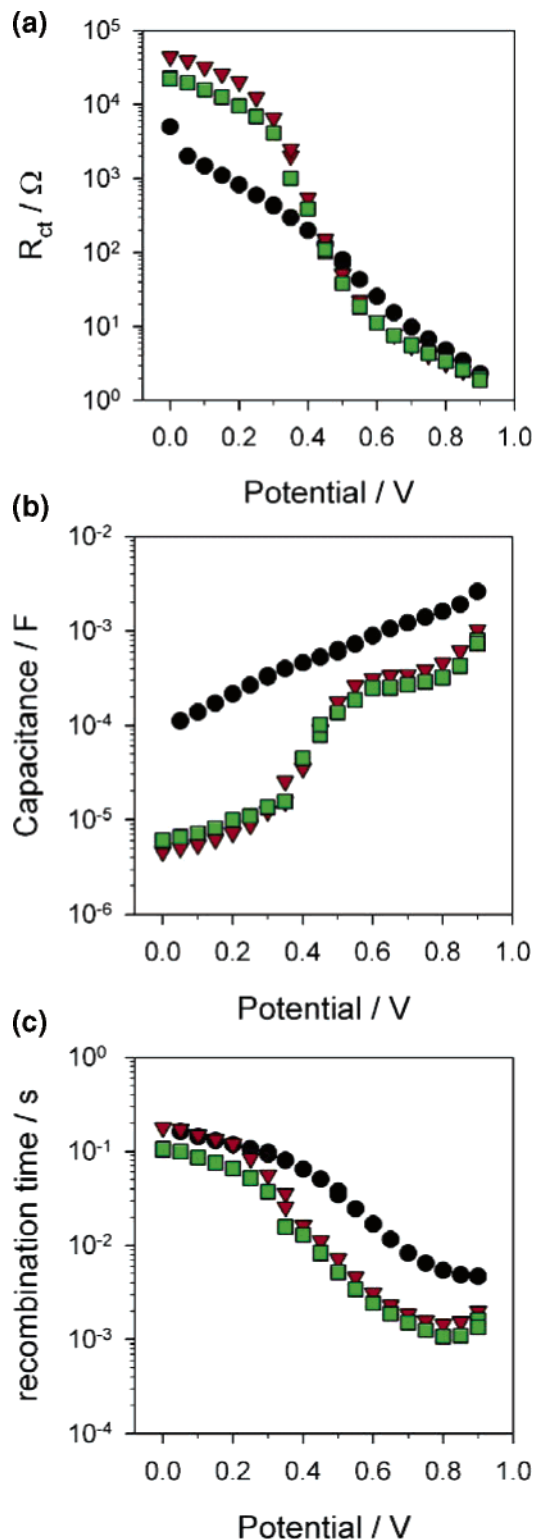
Figure 6. Values of the charge-transfer resistance (a), capacitance (b)c and recombination time (c) at liquid, C325 (black circles), and ionic electrolytes mixed C380 (red inverted triangles) and pure MPII C594 (green squares) cells under 1000 W m⁻² illumination with halogen lamp.

window of potentials to obtain information about the relative position of the conduction band.[23] Results for R_t from the fit to the transmission line model in Figure 4a are plotted in Figure 7b indicating that ionic liquid samples have their conduction band at nearly the same place, while the liquid cell has it approximately at a 50 mV smaller potential.

The much higher capacitance found for the organic solvent-containing electrolyte compared to the ionic liquids, Figure 6b
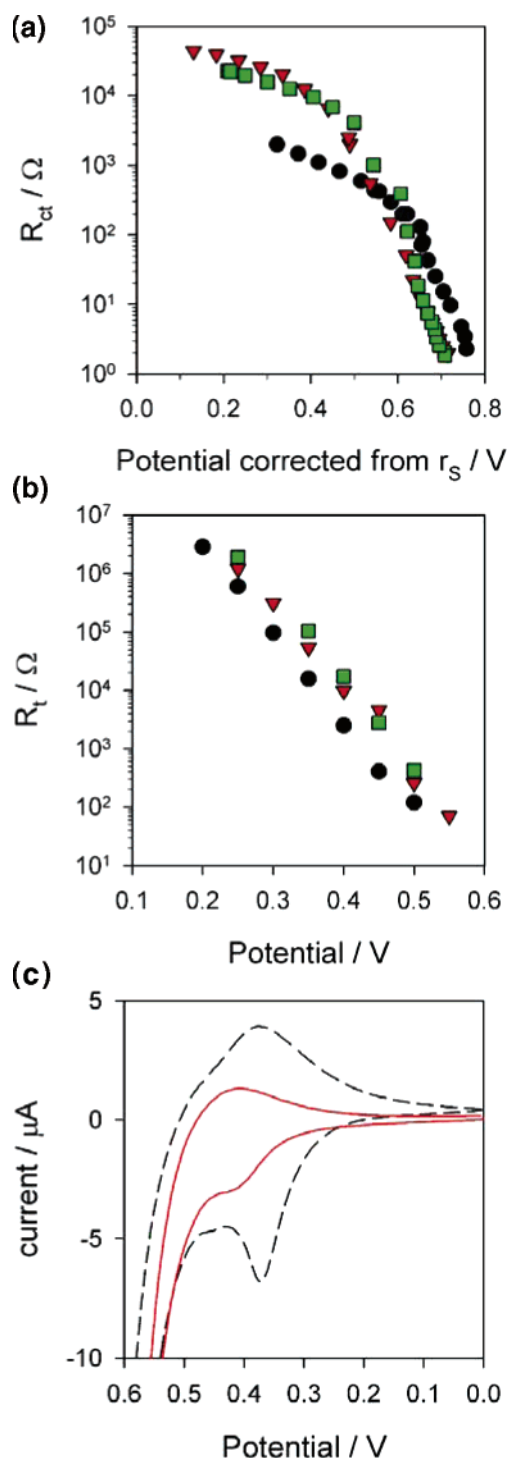
Figure 7. (a) Recombination resistances of Figure 6a after series resistance correction. Despite previous result, onset of R_{ct} starts at more negative potentials in the case of liquid cell. (b) Transport resistance evolution for liquid electrolyte (black circles), and molten salt electrolytes mixed C380 (red inverted triangles) and pure MPII C594 (green squares) samples in the dark. Conduction band in liquid cell is at 50 mV lower potential. (c) Cyclic voltammetry in the dark showing localized intraband state for liquid electrolyte cell (black dashed line) and for mixed ionic liquid electrolyte (red solid line). The shape of the peak during the reverse bias indicates little recombination.

indicates a higher density of accessible electronic states within the film or at the interface. The capacitance of the film at the potentials presented is given by the sum of the capacitance at the interface and the chemical capacitance of the film given by[23,32]

$$C_\mu = \frac{e^2}{k_B T} \exp\left[\frac{\alpha}{k_B T}(E_{Fn} - E_{cb})\right] \tag{5}$$

where E_{cb} is the energy of the conduction band and α is a constant related to the distribution of electronic states below the conduction band.[32] Part of this capacity increase is thus caused by the downward shift in the conduction band position, which agrees with the larger short circuit current observed with these cells, as shown in Table 1.

Additional capacitance contributions may be introduced by localized electronic states in the $TiO_2{}^\bullet$, as pointed out by the peaks in the cyclic voltammogram appearing at around 0.4 V. The intensity and reversibility of the peaks is influenced by both the $TiCl_4$ treatment and the solvent interaction with the surface. In our case, the slight displacement of the small bump of the C380 ionic liquid with respect to the big peak in liquid cell C325 agrees well with the band shift and a poorer $TiCl_4$ coating as described above.

The effect of this extra capacitance is clearly seen in the case of the impedances of the ionic liquid cells, as a large distortion from the expected exponential behavior due to the chemical capacitance of the charging of the exponential density of states in TiO_2. In the case of the liquid cell, however the capacitance is already so high that this contribution becomes negligible, although from the voltammetry data of the fresh sample we could expect it to be larger that in the ionic liquid case.

The product of the charge-transfer resistance and the chemical capacitance corresponds to the electron lifetime, $\tau = R_{ct}C_\mu$. From Figure 6c, τ is much larger for the solvent-containing electrolyte than for the ionic liquids especially at potentials close to the V_{oc}, and this is one of the reasons why photovoltaic performance of the former is superior to that of the latter cells. Electrolyte in C380 presents a slightly higher recombination time than in C594, which contributes to a higher efficiency of this cell.

These data, combined with the $i-V$ characteristics, give a detailed picture of the situation in the cell. In all cases, recombination time at short circuit is very similar and relatively high, even at 1 sun. However, the short circuit current is much higher in the liquid than in the ionic salt devices (Table 1). Two reasons may influence this result. On one hand, greater losses in the TiO_2 due to shorter diffusion length (Supporting Information, Figure S.2) and on the other, a lower injection from the dye due to either reductive quenching by iodide or the small shift in the conduction band.[35]
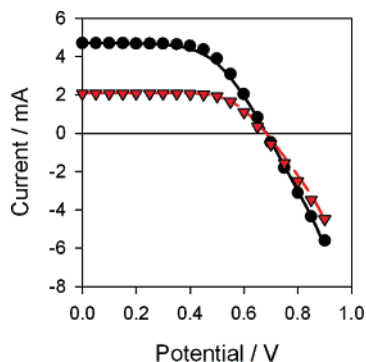
Evaluation of the impact of the resistances obtained from impedance measurements of the different cells may be done by analyzing their effect in the $i-V$ curve. Let us consider how to construct the $i-V$ curve starting from the different cell resistances. Taking into account that the total resistance is the sum of all the contributions, $R_{total} = R_{STCO} + R_c + R_{ct} + R_d$, and thus depend strongly on the potential, using the current at short circuit, I_{sc}, we can obtain the current crossing the sample at a certain potential through

$$i = -\int_0^V \frac{dV}{R_{total}} + I_{sc} \tag{6}$$

Alternatively, we can calculate the potential given by the cell (or necessary to apply to it) at a certain current from

$$V = -\int_{I_{sc}}^i R_{Total}\, di \tag{7}$$

Excellent agreement is found between the results from impedance and the original $i-V$ curve at the two illuminations applied over sample C594, as shown in Figure 8.

Impedance Spectroscopy of Dye-Sensitized Solar Cells

J. Phys. Chem. C, Vol. 111, No. 17, 2007 **6557**

Figure 8. *i*−*V* curves of sample C594 at 0.5 sun and 1 sun illumination (lines) and generated *i*−*V* curve from impedance data (dots). Excellent match is obtained.
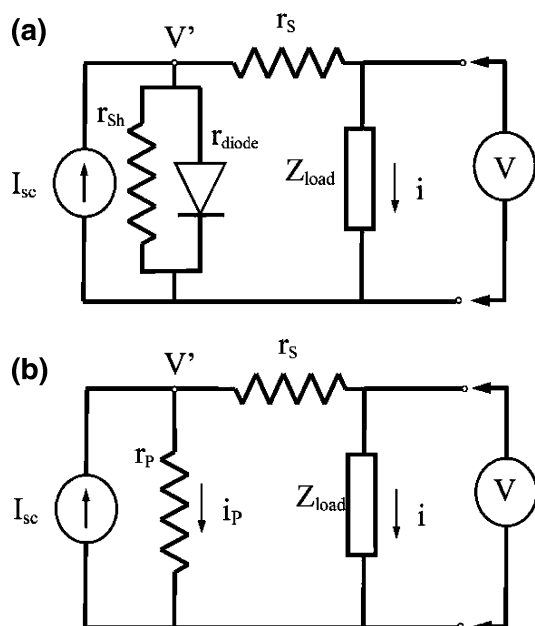

Figure 9. (a) Standard equivalent circuit for a solar cell. (b) Simplified equivalent circuit applied to DSC.

To explain the differences between the two *i*−*V* curves, we now have to adapt our equivalent circuit of ac impedance to the standard equivalent circuits used to study solar cells. The main elements in the steady-state equivalent circuit of a solar cell, shown in Figure 9a, are a current source accounting for electron injection from light, a series resistance accounting for contacts and wires, and a diode accounting for charge crossing the selective contact.[21] We may represent the diode as a resistance by the following:

$$r_{\text{diode}} = \frac{V'}{I_S\left(\exp\left[\dfrac{e}{mkT}V'\right] - 1\right)} \qquad (8)$$

where I_S is the saturation current of the junction, $V' = V + ir_S$ is the potential at the extreme of the diode, and m is the ideality factor of the diode. In many cases, a resistance in parallel to the diode, r_{shunt}, is added to account for charge losses near short circuit conditions that dominates the value of the parallel branch at low potentials.[21] To simplify the notation of this circuit, both r_{diode} and r_{shunt} may be substituted by an equivalent resistance, r_P, connected in parallel to the current source (Figure 9b).

Let us examine the influence of the different resistive elements in the solar cell characteristics. The model presents several behaviors depending on the values of r_S and r_P, as shown
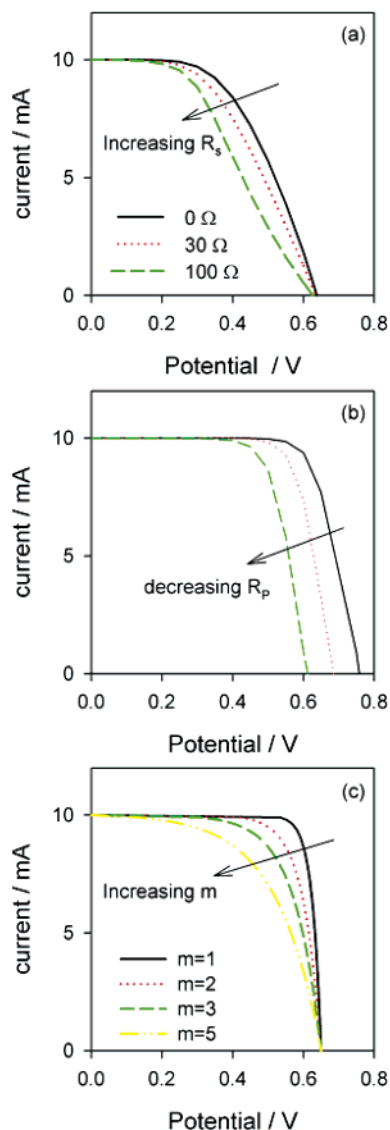
Figure 10. Evolution of simulated *i*−*V* curves with the change of overall series resistance (a), charge-transfer resistance (b), and ideality factor (c). Short circuit current is fixed at 10 mA.

in Figure 10. When r_S increases, the fill factor (FF) decreases while I_{sc} and V_{oc} remain constant,[21,25] diminishing the overall efficiency of the cell (Figure 10a). The transition of r_P from values dominated by r_{shunt} to values given by r_{diode}, which is controlled by I_S in eq 8, produces changes in V_{oc}. Therefore the sooner r_{diode} reaches low values, the smaller V_{oc} becomes (Figure 10b). The last parameter to be analyzed in this model is the ideality factor. At a given V_{oc}, the larger the m is, the lower the FF is (Figure 10c). This fact reduces the importance of the effect of R_S (Figure 10a), which is very strong when $m = 1$.[21]
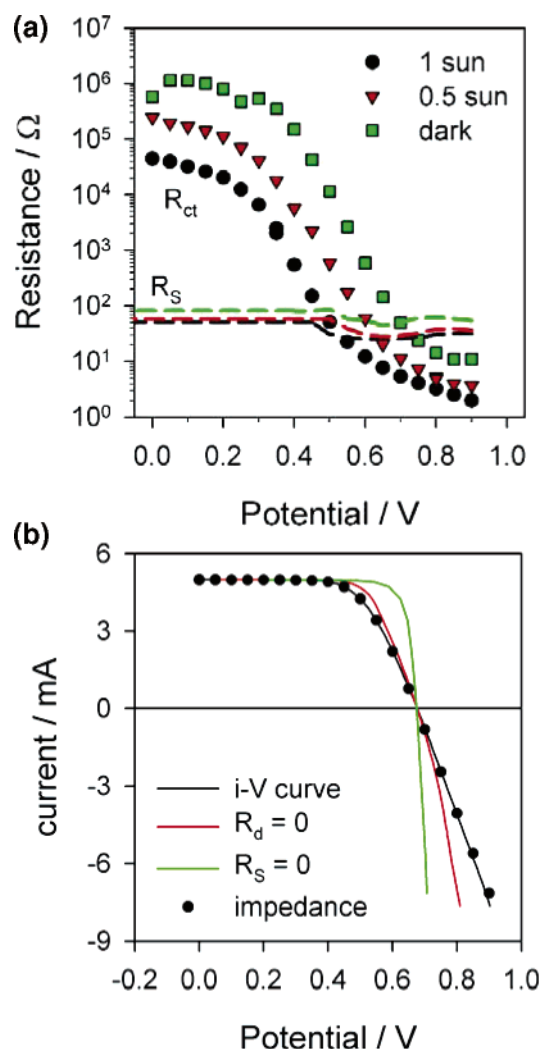
In the case of the DSC, the value of r_S is related with the total series differential resistance $R_S = R_{S_{TCO}} + R_c + R_d$ through the equation

$$r_S = \frac{1}{I_{sc} - i}\int_{I_{sc}}^{i} R_S\, di = \frac{1}{i_P}\int_0^{i_P} R_S\, di \qquad (9)$$

while the parallel resistance (electron losses due to the forward bias) is given b

$$r_P = \frac{1}{I_{sc} - i}\int_{I_{sc}}^{i} R_{ct}\, di = \frac{1}{i_P}\int_0^{i_P} R_{ct}\, di \qquad (10)$$

Figure 11. (a) Values of charge-transfer resistance (symbols) and series resistance (dashed lines) in C380 sample at different illumination conditions. Series resistance presents small variations with potential and is higher at the lower light intensity. For potentials smaller than 0.4−0.5 V, series resistance may only be estimated. (b) $i-V$ curve in this sample at 1000 W m^{-2} and simulations (dashed lines) for the cases without series resistance and diffusion resistance.

As we have seen, the charge-transfer resistance in eq 10 has an exponential behavior associated with the charge-transfer at the oxide/liquid interface (and not with the existence of a semiconductor p-n junction). In these interfaces, rather than the ideality factor, a transfer factor $\beta = 1/m$ is used. In our case, after the r_S drop correction, we have found $\beta = 0.78$ ($m = 1.3$) for liquid ionic cells, and $\beta = 0.70$ ($m = 1.4$), which are better than the previously reported value of $\beta = 0.5$ ($m = 2$).[23]

The use of integrated resistances, Figure 11a, allows us to interpret the differences between the $i-V$ curves in Figure 8. The decrease in R_d and R_c at different illumination intensities reduces the value of r_S providing the small change observed in the slope of the curve $i-V$ at potentials near the open circuit. This effect facilitates maintaining a high FF, despite the increase in the current passing through the cell at higher illumination intensities. However, this compensation is small due to the fact that the larger differential resistance, $R_{STCO} = 16 \, \Omega$ remained constant. In Figure 11b, we have plotted the $i-V$ curve for C380 and simulated the $i-V$ curves that could be obtained after eliminating only the diffusion resistance (red line) or the total series resistance (green line). In the first case, FF increases 9%,
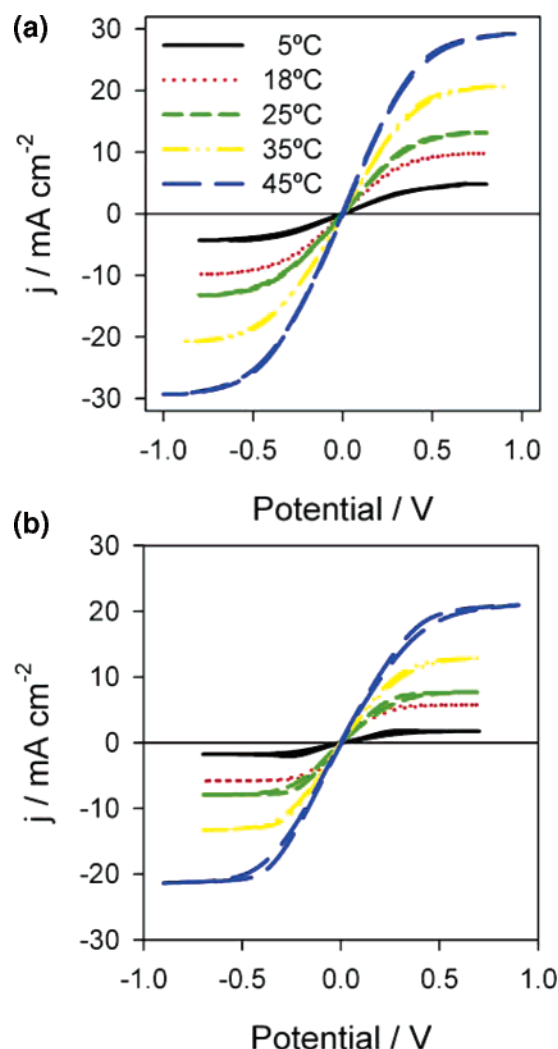
Figure 12. Changes in current limit in blank, ionic liquid, symmetric samples P380 (a), and P594 (b) due to temperature.

TABLE 3: Evolution of Diffusion Coefficient and Resistance (at 0.1 V) for the Two Ionic Liquids at Different Temperatures

temperature	D_{P594} (cm^2 s^{-1})	D_{P380} (cm^2 s^{-1})	$R_{d\,P594}$ (Ω)	$R_{d\,P380}$ (Ω)
5 °C	0.7×10^{-7}	1.3×10^{-7}	73	42
18 °C	1.5×10^{-7}	2.8×10^{-7}	25	16
25 °C	2.0×10^{-7}	3.4×10^{-7}	14	12
35 °C	3.4×10^{-7}	5.6×10^{-7}	7	7
45 °C	5.6×10^{-7}	7.9×10^{-7}	4	4

while in the second case the improvement is 28%. The main contribution to the reduction in FF (15%) has to be attributed to R_{STCO}.

It should also be mentioned that in the case of low-working temperatures, limitations to transport may occur due to the decrease of diffusion coefficient and increase in diffusion resistance, yielding to lower FF. This is seen in Figure 12 that shows the evolution of diffusion-limited current with the temperature for the symmetric blank cells. From these data, the diffusion coefficient could be calculated at the different temperatures, as shown in Table 3.

The strong dependence on temperature of diffusion resistance is plotted in Figure 13. Together with the effect of temperature, the increase of the resistance at higher voltages (currents) is again obtained as in Figure 1. Data in Table 3 reveals that despite the difference in diffusion coefficients, at high temper-
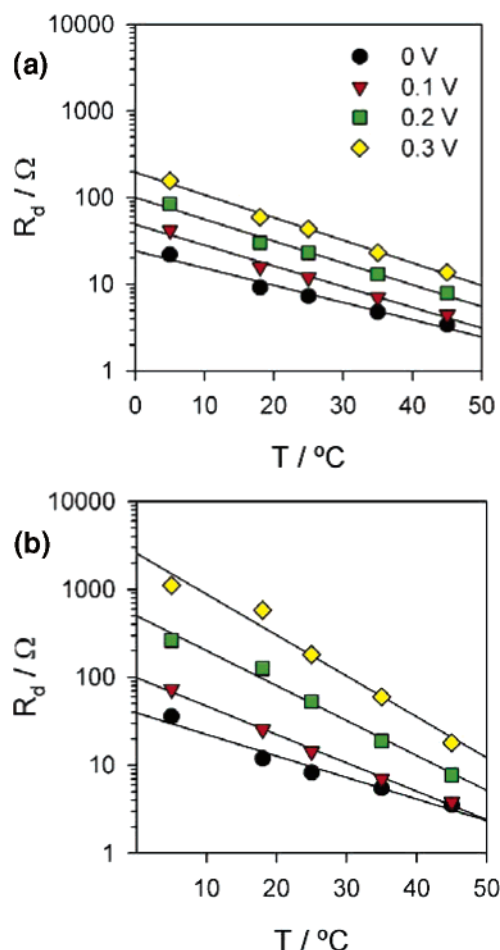
Figure 13. Evolution of diffusion resistance with temperature at different applied potentials for blank, ionic liquid, symmetric samples P380 (a), and P594 (b). At 5 °C, the resistance becomes large, especially in the case of the pure electrolyte Z594.

atures the two liquid electrolytes present the same values of diffusion resistance while at low temperatures these values diverge. This result agrees with the ones obtained in the dark and under illumination for complete cells in Figure 5. Comparison between data from Tables 2 and 3 allows us to estimate the temperature inside the cells under the illumination conditions.

As mentioned above, increasing the illumination has the effect of reducing R_{ct} (and thus r_P) (Figure 3b). As a consequence, V_{oc} reduces from the value that could be obtained if this effect would not occur (see Figure 10b), and the difference between V_{oc} at 500 and 1000 W m^{-2} illumination becomes small.

The differences found for the values of V_{oc} of the different samples also agree with the results in Figure 10b. The shift in the onset of R_{ct} from TiO$_2$ at lower values of potentials (Figure 7a) for the cases of ionic liquid, determines the onset of current recombination, contributing to a decrease of the photovoltage obtained for these cells with respect to the liquid sample, despite the higher position of their conduction band.

Impedance data suggest that improvement of the liquid ionic DSCs may be done in two ways:

• Reducing the series resistance. The dominant contribution of this resistance, $R_{S_{TCO}}$, may be diminished by two means: (i) using a lower sheet resistance glass that at least keeps the same level of transparency and (ii) improving the cell geometry and contacts with a better design. The improvement of R_d may be achieved by using a spacer as small as the TiO$_2$ layer or diminishing the viscosity of the electrolyte. To reduce R_{co}, a

better understanding of the TiO$_2$/TCO layer is needed. For R_{Pt}, an increase of the effective surface of Pt at counter electrode (i.e., by using a rough layer) may diminish the value of this resistance.

• Increasing the parallel resistance, which requires a reduction of recombination, or even better, shifting the onset of the exponential decrease in $R_{ct_{TiO2}}$ toward higher potentials. Both aspects may be achieved at the same time by covering TiO$_2$ with an insulating layer as Al$_2$O$_3$.[36] Further reductions of the charge-transfer resistance may be obtained by decreasing I$_3^-$ concentration to a level compatible with the diffusion of holes in the electrolyte and by diminishing the film thickness. This last procedure demands the use of higher extinction coefficient dyes than the ones used here to avoid a decrease in the absorption of the incident light.

4. Conclusions

The characteristics of several configurations of dye-sensitized solar cells have been studied by ac impedance and steady-state methods. The effect of recombination and series resistances on the photovoltage and FF of the DSC have been studied in detail and related with standard models for semiconductor solar cells.

Differences between the efficiency of a DSC with an ionic liquid as electrolyte and with a solvent-containing electrolyte have been found to be: (i) The lower injection of electrons from the dye to the TiO$_2$ that may be due to I$_3^-$ competitive absorption of light, smaller dye regeneration with I$^-$, larger self-recombination in the dye, and a small shift in the conduction band position with ionic liquid electrolyte. (ii) The smaller open circuit photopotential given by both the smaller electron injection and smaller onset potential of R_{ct} in liquid ionic cells that yield also to a higher recombination time at TiO$_2$/electrolyte surface. (iii) A larger diffusion resistance in the RTIL than in the liquid electrolyte. (iv) A larger transfer factor in the case of ionic electrolyte that improves the fill factor of the cell.

The main limiting factors in the RTIL dye solar with respect to liquid solvent cell are the higher recombination and lower injection of charge. Meanwhile, the differences in diffusion resistances of liquid and ionic liquid play a minor role in this case, provided that TCO resistance in operating conditions is always larger and dominates the series resistance in both kind of cells. However, at low temperatures the diffusion resistance in the ionic liquid cells may be the main limiting factor through its effect on the FF.

Without changing the basics of the presented RTIL-based DSCs, efficiency may be enhanced by reducing the different components of the series resistance of the cell; glass resistance is responsible of a 15% loss in the efficiency of present cells. Further improvements may be attained by optimizing cell thickness and counter electrode geometry.

Supporting Information Available: In this section, we provide (i) an example of the fit of a blank cell; (ii) some comments on the values of diffusion length of the different DSCs studied; and (iii) the relationship between diffusion resistance and viscosity. This material is available free of charge via the Internet at http://pubs.acs.org.

References and Notes

(1) O'Regan, B.; Grätzel, M. *Nature* **1991**, *353*, 737.

6560 *J. Phys. Chem. C, Vol. 111, No. 17, 2007*

Fabregat-Santiago et al.

(2) Nazeeruddin, M. K.; De Angelis, F.; Fantacci, S.; Selloni, A.; Viscardi, G.; Liska, P.; Ito, S.; Takeru, B.; Gratzel, M. *J. Am. Chem. Soc.* **2005**, *127*, 16835.

(3) Chiba, Y.; Islam, A.; Watanabe, Y.; Komiya, R.; Koide, N.; Han, L. *Jpn. J. Appl. Phys.* **2006**, *45*, L638.

(4) Hagfeldt, A.; Grätzel, M. *Acc. Chem. Res.* **2000**, *33*, 269.

(5) Grätzel. *J. Photochem. Photbiol., A* **2004**, *164*, 3.

(6) Tennakone, K.; Bandaranayake, P. K. M.; Jayaweera, P. V. V.; Konno, A.; Kumara, G. R. R. A. *Physica E* **2002**, *14*, 190.

(7) Bach, U.; Lupo, D.; Comte, P.; Moser, J. E.; Weissörtel, F.; Salbeck, J.; Spreitzer, H.; Grätzel, M. *Nature* **1998**, *398*, 583.

(8) Krüger, J.; Plass, R.; Cevey, L.; Piccirelli, M.; Grätzel, M.; Bach, U. *Appl. Phys. Lett.* **2001**, *79*, 2085.

(9) Gebeyehu, D.; Brabec, C. J.; Sariciftci, N. S.; Vangeneugden, D.; Kiebooms, R.; Vanderzande, D.; Kienberger, F.; Schindler, H. *Synth. Met.* **2002**, *125*, 279.

(10) Cao, F.; Oskam, G.; Searson, P. C. *J. Phys. Chem. B*, **1995**, *99*, 17071.

(11) Wang, P.; Zakeeruddin, S. M.; Moser, J.-E.; Grätzel, M. *J. Phys. Chem. B* **2003**, *107*, 13280.

(12) Kubo, W.; Kambe, S.; Nakade, S.; Kitamura, T.; Hanabusa, K.; Yanagida, S. *J. Phys. Chem. B* **2003**, *107*, 4374.

(13) Wang, P.; Zakeeruddin, S. M.; Humphry-Baker, R.; Grätzel, M. *Chem. Mater.* **2004**, *16*, 2694.

(14) Bonhôte, P.; Dias, A.-P.; Papageorgious, N.; Kalyanasundaraman, K.; Grätzel, M. *Inorg. Chem.* **1996**, *35*, 1168.

(15) Welton, T. *Chem. Rev.* **1999**, *99*, 2071.

(16) Lagrost, C.; Carrié, D.; Vaultier, M.; Hapiot, P. *J. Phys. Chem. A* **2003**, *107*, 745.

(17) Hagiwara, R.; Ito, Y. *J. Fluorine Chem.* **2000**, *105*, 221.

(18) Randriamahazaka, H.; Plesse, C.; Teyssié, D.; Chevrot, C. *Electrochem. Commun.* **2004**, *6*, 299.

(19) Buzzeo, M. C.; Evans, R. G.; Compton, R. G. *ChemPhysChem* **2004**, *5*, 1106.

(20) Fabregat-Santiago, F.; Randriamahazaka, H.; Zaban, A.; Garcia-Cañadas, J.; Garcia-Belmonte, G.; Bisquert, J. *Phys. Chem. Chem. Phys.* **2006**, *8*, 1827.

(21) Sze, S. M. *Physics of Semiconductor Devices*, 2nd ed.; John Wiley and Sons: New York, 1981.

(22) Hoshikawa, T.; Kikuchi, R.; Eguchi, K. *J. Electroanal. Chem.* **2006**, *588*, 59.

(23) Fabregat-Santiago, F.; Bisquert, J.; Garcia-Belmonte, G.; Boschloo, G.; Hagfeldt, A. *Sol. Energy Mater. Sol. Cells* **2005**, *87*, 117.

(24) Koide, N.; Han, L.; Chiba, Y.; Mitate, T. *Appl. Phys. Lett.* **2004**, *84*, 2433.

(25) Han, L.; Koide, N.; Chiba, Y.; Islam, A.; Komiya, R.; Fuke, N.; Fukui, A.; Yamanaka, R. *Appl. Phys. Lett.* **2005**, *86*, 213501.

(26) Wang, Q.; Ito, S.; Grätzel, M.; Fabregat-Santiago, F.; Mora-Seró, I.; Bisquert, J.; Bossho, G.; Imai, H. *J. Phys. Chem. B* **2006**, *110*, 19406.

(27) Kuang, D.; Ito, S.; Wenger, B.; Klein, C.; Moser, J.-E.; Humphry-Baker, R.; Zakeeruddin, S. M.; Grätzel, M. *J. Am. Chem. Soc.* **2006**, *128*, 4146.

(28) Hauch, A.; Georg, A. *Electrochim. Acta* **2001**, *46*, 3457.

(29) Greef, R.; Peat, R.; Peter, L. M.; Pletcher, D.; Robinson, J. *Instrumental Methods Electrochemistry*; Ellis Horwood Ltd: Chichester, England, 1985.

(30) Macdonald, J. R. *Impedance Spectroscopy*; John Wiley and Sons: New York, 1987.

(31) Hauch, A.; Georg, A.; Baumgärtner, S.; Opara-Krasovec, U.; Orel, B. *Electrochim. Acta* **2001**, *46*, 2131.

(32) Bisquert, J. *Phys. Chem. Chem. Phys.* **2003**, *5*, 5360.

(33) Huddleston, J. G.; Visser, A. E.; Reichert, W. M.; Willauer, H. D.; Broker, G. A.; Rogers, R. D. *Green Chem.* **2001**, *3*, 156.

(34) Wang, Q.; Ito, S.; Grätzel, M.; Fabregat-Santiago, F.; Mora-Seró, I.; Bisquert, J.; Bossho, T.; Imai, H. *J. Phys. Chem. B* **2006**, *110*, 25210.

(35) Wang, P.; Bernard.; Humphry-Baker, R.; Moser, J. E.; Joel, T.; Kantlehner, W.; Mezger, J.; Stoyanov, E. V.; Zakeeruddin, S. M.; Grätzel, M. *J. Am. Chem. Soc.* **2005**, *127*, 6850.

(36) Palomares, E.; Cliffort, J. N.; Haque, S. A.; Lutz, T.; Durrant, J. R. *J. Am. Chem. Soc.* **2003**, *125*, 475.

Correlation between photovoltaic performance and impedance spectroscopy of dye sensitized solar cells based on ionic liquids

Francisco Fabregat-Santiago* [a], Juan Bisquert [a], Emilio Palomares [b], Luis Otero [c], Daibin Kuang [d], Shaik M. Zakeeruddin [d], Michael Grätzel* [d]

[a] Departament de Ciències Experimentals, Universitat Jaume I, 12071 Castelló, Spain
[b] Institut Català d'Investigació Química, Av. Països Catalans 16, 43007 Tarragona, Spain
[c] Departamento de Química, Universidad Nacional de Río Cuarto, Agencia Postal 3 (5800), Río Cuarto, Argentina,
[d] Laboratory for photonics and interfaces, Institute of Chemical Sciences and Engineering, Ecole Polytechnique Federale de Lausanne, 1015 Lausanne, Switzerland.
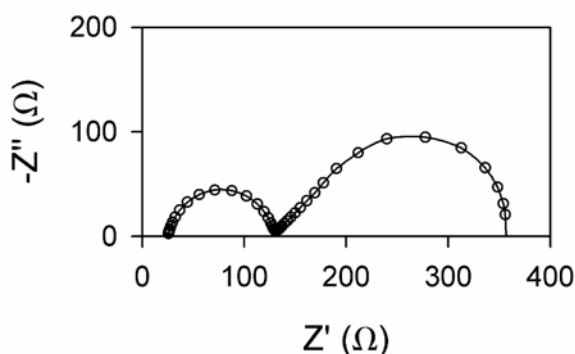
Fit of blank cell

Fig. S.1 : Experimental impedance (û)and fit (—) data of Z594 blank cell at 1 V.

In the region where the diffusion is relevant in the impedance spectrum, data fit very well to a Randles Circuit, Fig. 3(a)
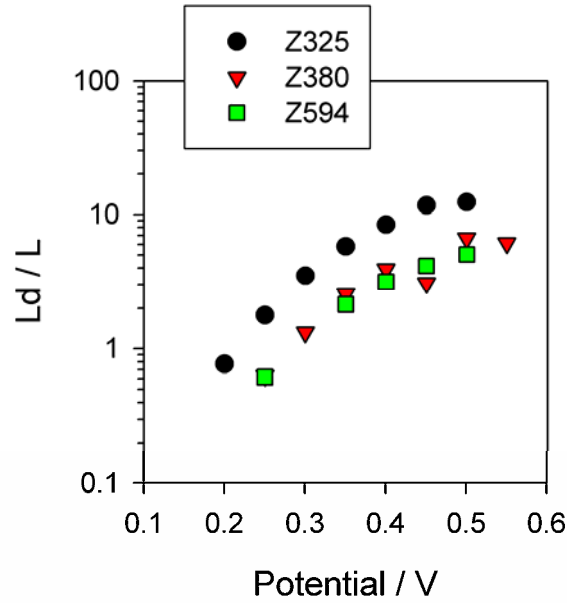
Diffusion length aspects

Fig. S.2 : Normalized effective diffusion length of DSSC's with different electrolytes in the dark.

The shift of the diffusion length found for liquid and ionic salts is not fully explained by the shift in the conduction band, Fig. 7(b). Thus higher recombination along the TiO_2 film at low potentials or lower light injection are needed to understand the smaller short circuit current found for the ionic liquid cells, Table I.

Relationship between diffusion resistance and viscosity

Viscosity has a strong dependence on temperature given by Vogel-Tamman-Fulcher equation [1]

$$\eta = \eta_0 \exp\left[B/(T-T_0)\right] \tag{S1}$$

where B, η_0 and T_0, are constants and T is the temperature.
Considering Stokes-Einstein relation

$$D = \frac{kT}{\pi \eta r} \tag{S2}$$

and taking the expression of the diffusion resistance [2, 3]:

$$R_d = \frac{L}{eSD}\left(\frac{dc}{dV}\right)^{-1} \tag{S3}$$

we obtain that the diffusion resistance depends on viscosity following:

$$R_d = \frac{L}{S} \frac{\pi\, r}{ekT} \left(\frac{dc}{dV} \right)^{-1} \eta \tag{S4}$$

with k Boltzman constant, r the effective hydrodynamic radius and c the ion concentration, e electron charge, L and S thickness and section of the cell and V the potential.

In the case of gradients of temperature, calculation of effective diffusion resistance from viscosity becomes complicated. Assuming that the gradient is small and that dc/dV does not change, R_d may be estimated from the average viscosity temperature quotient.

$$R_d = \frac{L}{S} \frac{\pi\, r}{ek} \left(\frac{dc}{dV} \right)^{-1} \frac{\overline{\eta}}{\overline{T}} \tag{S5}$$

Little gradients are expected in a 20µm cavity working in steady state conditions.

References:

[1] A. Noda, K. Hayamizu, M. Watanabe, J. Phys. Chem. B 2001, **105**, 4603-4610
[2] C. Ho, I.D. Raistrick and R.A. Huggins, J. Electrochem. Soc. 1980, **127,** 343-350
[3] J. Bisquert, G. Garcia-Belmonte, F. Fabregat-Santiago and P. Bueno, J. Electroanal. Chem. 1999, **475**, 152–163